Confined nematic liquid crystal between two spherical boundaries with planar anchoring

Seyed Reza Seyednejad,[1] Mohammad Reza Mozaffari,[2,*] and Mohammad Reza Ejtehadi[1,†]
[1]*Department of Physics, Sharif University of Technology, P.O. Box 11155-9161, Tehran, Iran*
[2]*Department of Physics, University of Qom, P.O. Box 3716146611, Qom, Iran*
(Received 22 March 2013; published 30 July 2013)

Nematic shells of liquid crystals have been provided in microscales. Defect structures in the shells are very essential in the electro-optical applications of such colloidal objects. We have numerically minimized the free energy of symmetric and asymmetric spherical shells of the nematic liquid crystal. Considering degenerate planar anchoring on the surfaces and isotropic nematic elasticity, a variety of defect structures are observed by controlling or varying the thicknesses of the shell and its degree of asymmetry. In symmetric shells, our calculations show that boojums (bipolar) defects appear in thick shells and tetrahedral (baseball) defects in thin shells. In asymmetric shells, while we are in the bipolar regime, the boojums defects transform to trigonal configurations. Free energy landscape shows that in this regime the inner droplet is not stable in the center and it is trapped in an off-center minimum energy position. For the case of thin shells, there are two degenerate director textures with similar tetrahedral configuration of the disclination lines. The levels are split in asymmetric shells. The stability of the inner droplet in the center position depends on director texture. It is stable for one texture and unstable for the other one. For an unstable pattern there is no minimum energy position for the inner droplet and it moves until it touches the outer boundary.

DOI: 10.1103/PhysRevE.88.012508 PACS number(s): 61.30.Hn, 61.30.Jf, 61.30.Pq, 64.70.pv

I. INTRODUCTION

Competition between elastic properties and boundary conditions of the nematic liquid crystals (NLC), confined between two spherical geometries, leads to beautiful topological defect textures [1–5]. Such nematic shells, which are experimentally made by double-emulsion techniques in microfluidic devices [1,2,6], have potentially provided for electro-optic applications [3,4] and microscale colloidal linkers [7]. The spatial distribution of the defect textures completely depends on the shell thickness and the anchoring of the director on the boundaries [1,8]. A number of interesting states occur when one or both of the boundaries have planar anchoring [9,10]. Here we concentrate on the study of degenerate planar anchoring on both surfaces. The equilibrium defect arrangements are determined by the minimization of the elastic free energy in the presence of the surface boundary conditions [11]. The induced topological charges which are the main reason for the director disagreement in the bulk and on the surfaces, are specified by the amount of the director rotation about the defect core. According to the Poincare-Hopf theorem, the total topological charge on a spherical nematic drop with planar anchoring is equal to $+2$ [12,13]. There are two main defect arrangements as a function of thickness in symmetric shells. They are two pairs of boojums ($s = +1$) at the north and south poles and four disinclination line defects ($s = +1/2$) at the vertices of a tetrahedron [1,3,8], respectively. It has been experimentally understood that the boojums defects take place in thick shells and the tetrahedral defects appear in thin shells [1]. There is a crossover between their free energies which specifies the final defect arrangement as a function of thickness [4]. A Monte Carlo study shows that applying homogeneous external fields provide a transition from a four disinclination line defect to a two pair boojums structure, and at inhomogeneous external fields, the complicated defect arrangements appear in the shell that may have positive and negative topological charges [14]. In the thin shells, provided that the bend elastic constant K_{bend} is larger than the splay elastic constant K_{twist}, the tetrahedral line defects are rearranged on a great circle [9,15].

Fernandez-Neives and co-workers experimentally show that the inner droplet with nearly constant velocity moves to the outer surface and does not keep its spherical distribution [1]. They argued that the balance between the elastic properties and the media drag forces specifies the particle motion [8]. This behavior takes place in both boojums and tetrahedral defect textures. In the two pair boojums case, the inner droplet displaces along the line joining the boojums defects [1]. Recent free energy minimization of a thin shell has explained that due to a small negative slope in the media elastic potential about the symmetric situation, the inner droplet moves out, even in the absence of the buoyancy forces [9]. In tetrahedral regimes, the elastics distortions and the defect textures are limited to the thinner part of the nematic shell [3,8,9].

In asymmetric geometries, the director distortions can induce a wide range of defect textures dependent on the thickness of the shell and properties of the nematic elasticity [2,3,8,9]. One of them is characterized by two defects $s = +1/2$ and a defect $s = +1$ where they are geometrically introduced as an isosceles triangle in the shell [3,8]. Their equal angles that contain $s = +1/2$ defects are spatially distributed in the thinnest area. Another defect ordering includes two $s = +1$ [3]. Although the accumulation of the defects in the thin part of the nematic shell decreases the cost of the elastic energy, the repulsion between defects prevents coalescence [14,16].

In this paper we numerically study the topological defect textures in the spherical NLC shells by minimizing the sum of elastic Landau–de Gennes free energy and the planar

*m.mozaffari@qom.ac.ir
†ejtehadi@sharif.physics.edu

degenerate surface energy introduced by Fournier and Galatola. We investigate the behavior of defects at different spatial arrangements of the inner droplet in the shell.

II. THE MODEL

The geometry of the studied system is schematically illustrated in Fig. 1(a). We consider a confined nematic shell between two spherical surfaces. The shell radii in the inner and outer boundaries are a and R, respectively. We scale all the lengths with respect to the outer shell radius R. The line joining the center of the spheres is given by Δ and the shell thickness is defined by $h = R - a$ at the $\Delta = 0$.

A local traceless and symmetric tensor order parameter $Q_{ij} = S(\hat{n}_i\hat{n}_j - \delta_{ij}/3)$ can describe the nematic order in confined media, in which the scalar order parameter S and the director orientation $\hat{n}$ are determined by the largest eigenvalue $\lambda_{\max} = \frac{2}{3}S$, and its corresponding eigenvector of the tensor Q, respectively. Here we use the tensor order parameter with six components Q_{xx}, Q_{xy}, Q_{xz}, Q_{yy}, Q_{yz}, and Q_{zz}, where $Q_{xx} + Q_{yy} + Q_{zz} = 0$. The director has degenerate planar anchoring on the shell boundaries. The equilibrium orientation of the director field is determined by balancing both bulk and surface properties of the director.

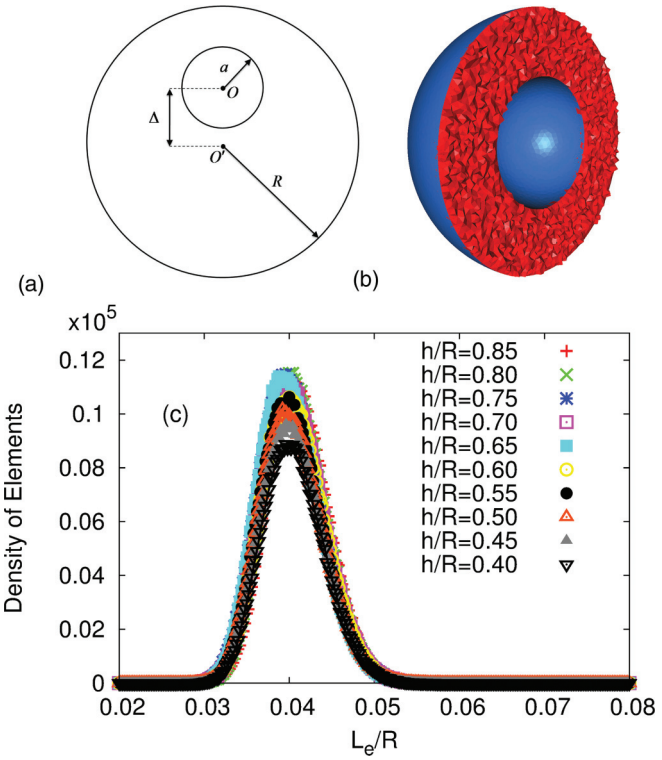

FIG. 1. (Color online) (a) A cross section of the 3D studied system, passing through the centers of inner (O) and outer (O') spheres. The nematic shell is confined between two spheres with radii a and R. $\Delta(=OO')$ is the distance between the centers of the spheres. (b) A typical tetrahedral mesh used in the FEM calculations. (c) The figure shows the size distribution of tetrahedral elements at different thicknesses $h(=R-a)$ in the symmetric shells ($\Delta = 0$), where the characteristic size of any tetrahedral element L_e is the size of a regular tetrahedral with equal volume.

A. The bulk free energy

The bulk free energy of the nematic fluid in the absence of the buoyancy forces is described well by the Landau–de Gennes model [17], in which the free energy functional is expanded in powers of the tensor order parameter and its spatial derivatives:

$$F_b = \int_\Omega dV \left[\frac{A}{2} Q_{ij}Q_{ji} - \frac{B}{3} Q_{ij}Q_{jk}Q_{ki} + \frac{C}{4}(Q_{ij}Q_{ji})^2 + \frac{L_1}{2}\partial_k Q_{ij}\partial_k Q_{ij} + \frac{L_2}{2}\partial_i Q_{ik}\partial_j Q_{jk} + \frac{L_3}{2} Q_{ij}\partial_i Q_{kl}\partial_j Q_{kl} \right], \quad (1)$$

where the indices refer to Cartesian coordinates, the summation over repeated indices is assumed, and Ω denotes the liquid crystal volume. The first three terms are the Landau–de Gennes free energy which describe the bulk isotropic-nematic (IN) transition. The coefficients A, B, and C are the material-dependent parameters.

The derivative terms are the contribution of the elastic free energy in the nematic phase. The nematic elastic constants L_1, L_2, and L_3 are related to the Frank elastic constants by $L_1 = (3K_{\text{twist}} - K_{\text{splay}} + K_{\text{bend}})/6S^2$, $L_2 = (K_{\text{splay}} - K_{\text{twist}})/S^2$, and $L_3 = (K_{\text{bend}} - K_{\text{splay}})/2S^3$.

In this study we restrict ourselves to an one-elastic constant approximation that means all the Frank elastic constants should be equivalent, which leads to L_2,$L_3 = 0$.

To simplify calculations we rescale the tensor order parameter as $q = (4B/3\sqrt{6}C)^{-1}Q$, such that $q_{ij} = \hat{S}(\hat{n}_i\hat{n}_j - \delta_{ij}/3)$, where $\hat{S} = (4B/3\sqrt{6}C)^{-1}S$. As a consequence, the dimensionless free energy becomes

$$\hat{F}_b = \frac{F_b}{f_0 R^3} = \int_\Omega \frac{dV}{R^3} \left[\frac{\tau}{2} q_{ij}q_{ji} - \frac{\sqrt{6}}{4} q_{ij}q_{jk}q_{ki} + \frac{1}{4}(q_{ij}q_{ji})^2 + \frac{1}{2}\xi^2 \partial_k q_{ij}\partial_k q_{ij} \right], \quad (2)$$

where $f_0 = C(4B/3\sqrt{6}C)^4$, $\tau = 27AC/8B^2$ is an effective dimensionless temperature, and $\xi = \sqrt{27L_1C/8B^2}$ is the nematic coherence length [18]. In this redefinition of parameters, the fluid undergoes a first-order isotropic-nematic transition at $\tau = 1/8$. The isotropic phase becomes unstable for $\tau < 0$. The scalar nematic order parameter in bulk is given by $\hat{S}_b = (3\sqrt{6}/16)(1 + \sqrt{1 - 64\tau/9})$. The dimensionless temperature and coherence length were set to $\tau = (3\sqrt{6} - 8)/12$ and $\xi/R = 0.0707$, respectively. This choice of parameters closely match the parameters of the widely used liquid crystal mesogen 5CB and results in formation of stable topological defects [18,19].

B. The surface free energy

The preferred anchoring can be modeled with much more ease [20,21] compared to the degenerate planar anchoring due to uniqueness of the orientation of nematic fluid in the vicinity of the surfaces. Fournier and co-workers [22] have introduced a two-parameter surface energy functional that is bounded from below and assumes its minimum in the manifold of degenerate planar configurations. The surface energy consists

of two terms, controlling the planar anchoring and fixing the scalar order parameter on the surface. Since we expect formation of topological surface defects, we relax the second constraint [19,23], resulting in the following single parameter surface energy functional:

$$F_s = W \int_{\partial\Omega} dA\,(\tilde{Q}_{ij} - \tilde{Q}^{\perp}_{ij})(\tilde{Q}_{ji} - \tilde{Q}^{\perp}_{ji}), \qquad (3)$$

where $\tilde{Q}_{ij} = Q_{ij} + S\delta_{ij}/3$, $\tilde{Q}^{\perp}_{ij} = (\delta_{ik} - \hat{\nu}_i\hat{\nu}_k)\tilde{Q}_{kl}(\delta_{lj} - \hat{\nu}_l\hat{\nu}_j)$ is the projection of $\tilde{Q}_{ij}$ onto the tangent plane of the surface, and $\hat{\nu}$ is the normal to the surface. The positive anchoring coefficient W controls the stiffness of anchoring. According to a dimensionless recipe in the bulk free energy subsection, the surface energy can be written in dimensionless variables as

$$\hat{F}_s = \frac{F_s}{f_0 R^3} = \frac{w}{R}\int_{\partial\Omega} \frac{dA}{R^2}\,(\tilde{q}_{ij} - \tilde{q}^{\perp}_{ij})(\tilde{q}_{ji} - \tilde{q}^{\perp}_{ji}), \qquad (4)$$

where $w = 27WC/8B^2$, $\tilde{q}_{ij} = (4B/3\sqrt{6}C)^{-1}\tilde{Q}_{ij}$, and $\tilde{q}^{\perp}_{ij} = (\delta_{ik} - \hat{\nu}_i\hat{\nu}_k)\tilde{q}_{kl}(\delta_{lj} - \hat{\nu}_l\hat{\nu}_j)$. We have set the anchoring length to $w/R = 0.3125$ [19,24], which is much larger than the coherence nematic length in this study. That means the choice leads to a strong degenerate anchoring of the 5CB mesogens on the surfaces.

III. NUMERICAL MINIMIZATION OF THE FREE ENERGY

We adopt a finite element method (FEM) to minimize the free energy functional, described in the preceding sections. As shown in Fig. 1(b), the nematic shell was decomposed into tetrahedral elements by using the automatic mesh generator Gmsh [25]. The tensor order parameter was linearly interpolated within each element of the mesh for the evaluation of the free energy integrals. The validity of linear interpolation depends on the order parameter deviations within each element. By diagonalization of the Hessian matrix, constructed by the order parameter, one can evaluate the mesh resolution [26]. Here we have manually arranged a series of the mesh adaptive runs, decreasing the mesh length size on the shell surfaces and minimizing the system free energy to evaluate the Hessian matrix. The mentioned procedure is repeated until the largest absolute eigenvalue of the Hessian is converged for any element. The size distribution of tetrahedral elements, in Fig. 1(c), shows that the size of the refined elements are small in comparison to the coherence length. For each configuration of the nematic shell (means for different a and Δ), the total dimensionless free energy $\hat{F}(=\hat{F}_b + \hat{F}_s)$ was minimized using a conjugate gradient (CG) method [27], where the minimization procedure was stopped when the relative free energy improvements dropped below 10^{-8}. We present and discuss the results in the next section.

IV. RESULTS AND DISCUSSION

To begin, we numerically study symmetric nematic shells ($\Delta = 0$) of different thicknesses $h(= R - a)$. In agreement with experimental observations [1,3], our calculations reveal two main defect configurations: (a) two pair boojums in thick shells and (b) tetrahedral structure in thin shells. As shown in Figs. 2(a) and 2(b), the defects of the thick shells are specified by two pairs of boojums of strength $s = +1$ at those poles of the two concentric spheres which are aligned along one of their common diameters. In thin shells, the tetrahedral structure, as shown in Figs. 2(c) and 2(d), is composed of four disclination line defects of strength $s = +1/2$ resembling sp^3 arrangement of the atomic bonds of diamond [3]. As one can see in Fig. 2(d), on both shell boundaries, the equilibrium director orientations exhibit baseball patterns [4].

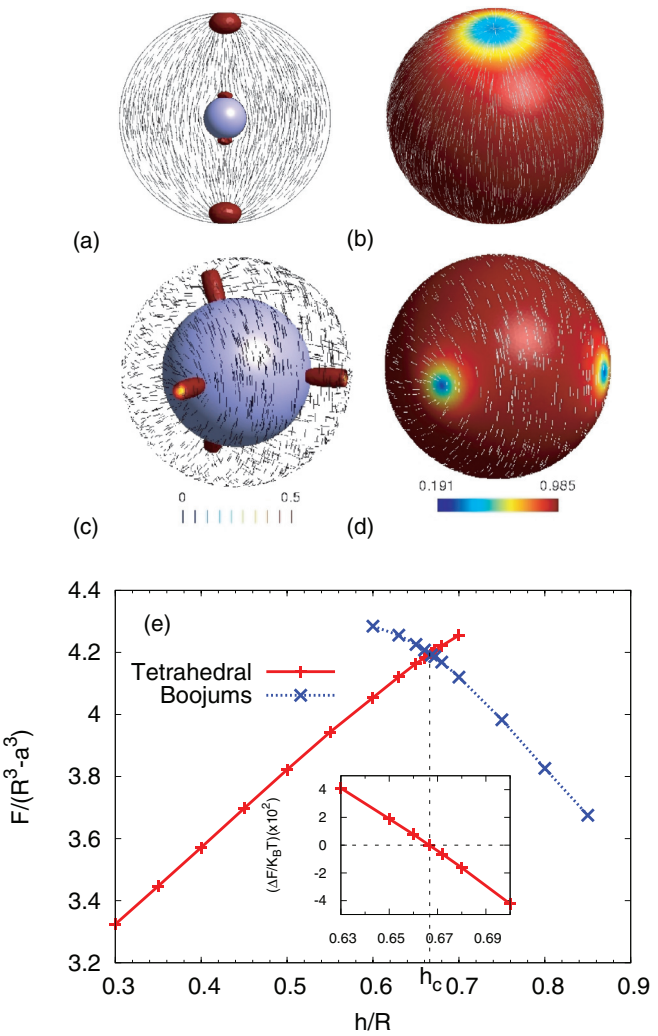

FIG. 2. (Color online) (a)–(d) Profiles of the scalar order parameter in the bulk and on the outer surface of nematic liquid crystal shells. Inside the bulk, anywhere the scalar order parameter is lower than $0.5\hat{S}_b$, is highlighted, which represents a topological defect. The director field has been specified by dashed lines. (a) and (b) Configurations with boojum defects for $h/R = 0.8$, and (c) and (d) are presenting configurations containing tetrahedral defects for $h/R = 0.35$. Free energy densities as a function of thickness of the shell, for both boojums and tetrahedral defect configurations, are presented in (e). The parameters are rescaled to be dimensionless (see text). The graph shows a level crossing on $h \approx h_c \sim 0.666R$. To zoom on a level crossing point, the region around the point has been scanned by higher resolution. The inset shows the energy difference between two energy levels $\Delta F = F_{\text{boojums}} - F_{\text{tetrahedral}}$ on this region.

We make an energy comparison between the boojums and the tetrahedral defect configurations. The dimensionless free energy densities (DFED) of both configurations $\hat{F}/(R^3 - a^3)$ in terms of the dimensionless thickness h/R are shown in Fig. 2(e). Gradually decreasing the symmetric shell thickness, an energy level crossing is observed in $h_c \sim 0.666R$, where the boojums defect structure undergoes a transition to the tetrahedral configuration. h_c marks the limit of stability for the boojums and the tetrahedral configurations, so that the boojum configurations appear in $h > h_c$ and the tetrahedral configurations in $h < h_c$. h_c is theoretically specified by the defect core radius r_c of the shells [4]. In our results, $\frac{r_c}{R}$ in the critical thickness h_c shows a small deviation from that reported in experiment, $1.47(\frac{r_c}{R})_{\text{expt}}$ [1]. Around the critical thickness, the energy difference between the boojums and the tetrahedral structures is a linear function of the shell thickness [see inset plot in Fig. 2(e)].

For the case of the asymmetric shells ($\Delta \neq 0$), which are constructed from eccentric spheres, we arrange a series of the free energy minimizations at different shell thicknesses ($h = R - a$) with respect to the degree of asymmetry Δ to determine an effective media elastic potential on the inner droplet. We see that the stability of the system is increased by getting more deviated from symmetric shell configurations. So the inner droplet tends to hold its center far from the the center of the outer sphere. The two different thickness limits $h > h_c$ and $h < h_c$ will be separately discussed.

For the case of $h > h_c$, the DFED of the system with respect to the scaled degree of asymmetry Δ/R is shown in Fig. 3(a). The droplet movement is performed along the diameter passing through the boojums defect cores of the symmetric shell state. Varying the shell degree of asymmetry, three different defect structures may be observed.

Our calculations show that the two pair boojums configurations can be maintained only for small deviations from symmetric shells. For thinner thicknesses of the asymmetric shell, the boojums configurations are less stable.

For large degrees of asymmetry, a new defect configuration appears which is characterized by two disinclination line defects ($s = +1/2$) and a pair of boojum defects ($s = +1$) on the opposite side [see Figs. 3(b) and 3(c)]. There are small discontinuities in the slope of the free energy which are related to rearrangement of the defects in the shell. The fracture is more visible for thicker shells.

For $h < 0.85R$, the inner droplet is running out of the center, but there is a minimum energy position in the free energy profile and rearrangement of the defects in the thinner side of the shell prevents the two spheres from touching each other. By going to thicker shells ($h \geqslant 0.85R$), the DFED slope indicates that the shell cannot preserve its stability, and the droplet reaches the outer wall, which is consistent with the experiments [1].

Focusing on the transition of the defect structures from boojums to trigonal texture, we see an unstable phase which is called a double-core boojum. As shown in Figs. 3(d) and 3(e), the double-core defect has been distributed on the outer boundary of the thinner part of the shell.

Starting from the boojums structure, the DFED has a very smooth peak at the $\Delta = 0$. Then, our calculations show in the absence of the buoyancy forces the symmetric position of the inner droplet is unstable.

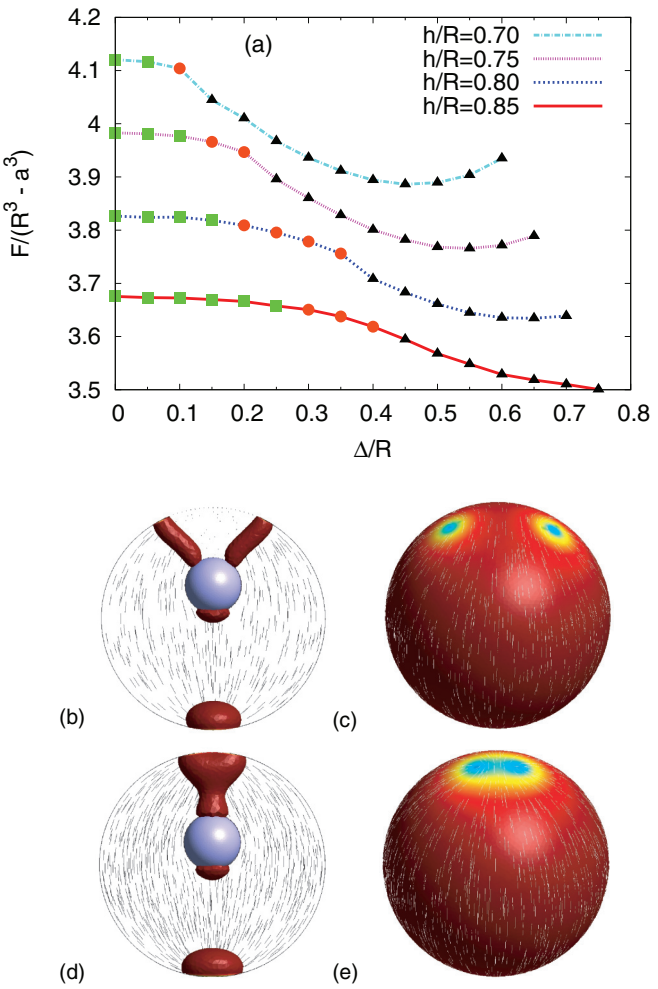

FIG. 3. (Color online) (a) The DFED for $h > h_c$ as a function of degree of asymmetry Δ/R. Square, circle, and triangle symbols correspond to the structures of boojums, transition state, and trigonal, respectively. (b)–(e) The scalar order parameter and related director field in the bulk and on the surfaces of the shell for $h/R = 0.75$. The trigonal defect is shown for $\Delta/R = 0.2$ (b) and (c), and the transition state (boojums-trigonal) for $\Delta/R = 0.3$ (d) and (e).

In the limit $h < h_c$, as it has been mentioned before, defects have tetrahedral structure in symmetric shells, but there are two possibilities for the director texture on the surface. One has a baseball pattern. If the director field is rotated locally by 90°, the other pattern is obtained which we call zonal. Both textures, which have been numerically obtained by different initial director orientations, are characterized by four disclination line defects ($s = +\frac{1}{2}$) and have equal energy in one constant approximation. This degeneracy has also been reported in [9]. For an asymmetric shell the degenerate level is split into two. For the baseball pattern, the free energy is higher than the symmetric configuration, which indicates that the pattern is a stable configuration [red dots in Fig. 4(a)]. For a zonal pattern, a pair of defects prefer to approach each other. The green curve in Fig. 4(a) shows the DFED of the system in this transition. The energy decreases by the degree of asymmetry. Thus the inner droplet is unstable at the $\Delta = 0$.

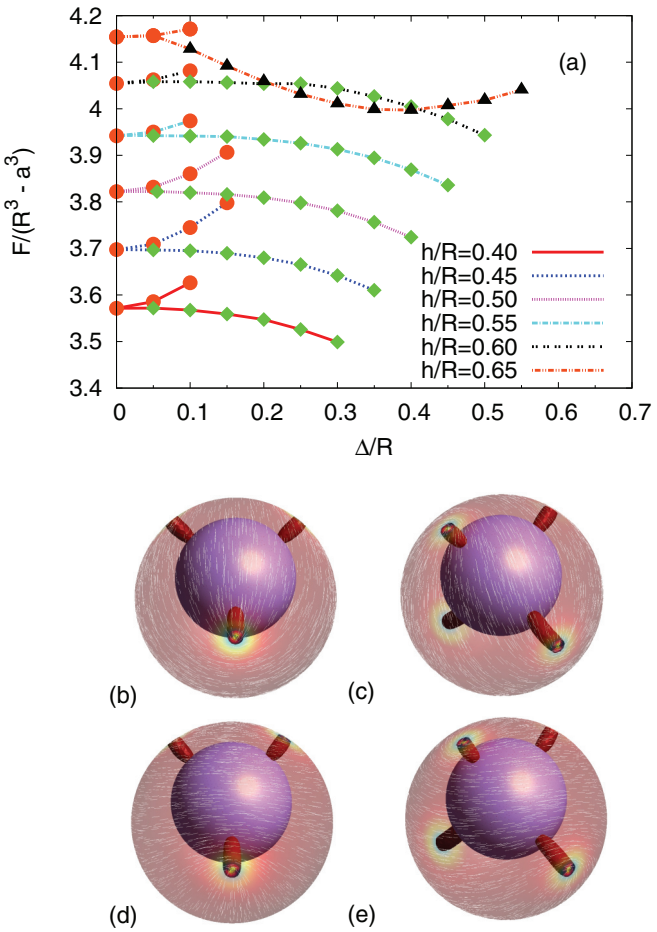

FIG. 4. (Color online) (a) The DFED for $h < h_c$ as a function of degree of asymmetry Δ/R. Diamond, circle, and triangle symbols correspond to the structures zonal-tetrahedral, baseball-tetrahedral, and trigonal, respectively. (b)–(e) Scalar order parameter and related director field in the bulk and on the surfaces of the shell for $h/R = 0.40$ and $\Delta/R = 0.15$. (b) and (c) A baseball pattern from two viewpoints and (d) and (e) similarly show a zonal pattern.

In contrast to the thick shells, there is no minimum in the energy profile of thin shells, and nothing prevents the inner droplet from touching the other surface.

V. SUMMARY

In summary, in this study the configuration of defects and the director patterns on a shell of nematic liquid crystal have been discussed. The shell is confined between two spherical boundaries. The surfaces have degenerate planar anchoring and one-constant approximation of the elastic energy is assumed.

Although it is simple to make a symmetric shell of the nematic medium on computer, it is not easy to keep the inner droplet in the center of the shell. Practically, due to buoyancy forces and also dynamics of defects, the droplet may run from the center and be trapped in a minimum free energy position. Here we have ignored buoyancy forces and, just by minimizing the free energy of the system, we have investigated defect structures of symmetric and asymmetric shells.

For the symmetric shell, where two boundaries are concentric, the defect structure depends on the thickness of the shell. For thick shells two pairs of boojums ($s = +1$) appeared across a diameter. By decreasing the thickness, the approaching boojums in a critical distance h_c transform to pairs of disclination lines ($s = +1/2$) and forms a sp^3-like structure. In this configuration of defects, according to numerical initial orientations, two different patterns of nematic texture (baseball or zonal) may be observed. Both have the same energy, thus, the ground state of the symmetric thin shell is degenerate.

By moving the inner droplet off the center, we have scanned the system free energy landscape for different degrees of asymmetry of the shell. As soon as the thickness of the shell in its thinner part passes critical thickness h_c, the boojums defects on that part transform to disclination lines and they arrange a trigonal configuration of defects. Free energy landscape shows that for this regime the inner droplet is not stable in the center and it is trapped in an off-center minimum energy position.

For the case of thin shells, by moving the inner droplet, the degenerate energy level of the symmetric shell is split into two separate levels. One has higher energy, which shows that the baseball state is stable as its energy is increased by degree of asymmetry. On the other hand, the zonal configuration is unstable and the droplet prefers to run off the center. In this case the free energy landscape does not show any minimum energy position, and the inner droplet moves until it touches the outer boundary.

ACKNOWLEDGMENTS

We would like to thank Masoomeh Hashemi for her very useful comments and reading the manuscript carefully. M.R.E also thanks T. Lopez-Leon, H.-L. Liang, and D. Sec for valuable discussions and comments.

[1] A. Fernández-Nieves, V. Vitelli, A. S. Utada, D. R. Link, M. Márquez, D. R. Nelson, and D. A. Weitz, Phys. Rev. Lett. **99**, 157801 (2007).
[2] T. Lopez-Leon and A. Fernandez-Nieves, Phys. Rev. E **79**, 021707 (2009).
[3] T. Lopez-Leon, V. Koning, K. B. S. Devaiah, V. Vitelli, and A. Fernandez-Nieves, Nat. Phys. **7**, 391 (2011).
[4] V. Vitelli and D. R. Nelson, Phys. Rev. E **74**, 021711 (2006).
[5] H.-L. Liang, S. Schymura, P. Rudquist, and J. Lagerwall, Phys. Rev. Lett. **106**, 247801 (2011).
[6] A. S. Utada, E. Lorenceau, D. R. Link, P. D. Kaplan, H. A. Stone, and D. A. Weitz, Science **308**, 537 (2005).
[7] D. R. Nelson, Nano Lett. **2**, 1125 (2002).
[8] T. Lopez-Leon and A. Fernandez-Nieves, Colloid Polym. Sci. **289**, 345 (2011).
[9] D. Sec, T. Lopez-Leon, M. Nobili, C. Blanc, A. Fernandez-Nieves, M. Ravnik, and S. Zumer, Phys. Rev. E **86**, 020705 (2012).
[10] M. A. Gharbi, D. Seč, T. Lopez-Leon, M. Nobili, M. Ravnik, S. Žumer, and C. Blanc, Soft Matter **9**, 6911 (2013).

[11] M. Kleman and O. D. Lavrentovich, *Soft Matter Physics: An Introduction* (Springer, Berlin, 2003).
[12] H. Poincare, J. Math. Pures Appl. **1**, 167 (1885).
[13] H. Hopf, Math. Ann. **96**, 427 (1926).
[14] G. Skacej and C. Zannoni, Phys. Rev. Lett. **100**, 197802 (2008).
[15] H. Shin, M. J. Bowick, and X. Xing, Phys. Rev. Lett. **101**, 037802 (2008).
[16] M. A. Bates, G. Skacej, and C. Zannoni, Soft Matter **6**, 655 (2010).
[17] P. G. de Gennes and J. Prost, *The Physics of Liquid Crystal* (Oxford University Press, New York, 1995).
[18] J.-i. Fukuda, H. Stark, M. Yoneya, and H. Yokoyama, Phys. Rev. E **69**, 041706 (2004).
[19] M. R. Mozaffari, M. Babadi, J.-i. Fukuda, and M. R. Ejtehadi, Soft Matter **7**, 1107 (2011).
[20] A. Rapini and M. Popoular, J. Phys. (France) **30**, 54 (1969).
[21] M. Nobili and G. Durand, Phys. Rev. A **46**, R6174 (1992).
[22] J. B. Fournier and P. Galatola, Europhys. Lett. **72**, 403 (2005).
[23] M. Vilfan, N. Osterman, M. Copic, M. Ravnik, S. Zumer, J. Kotar, D. Babic, and I. Poberaj, Phys. Rev. Lett. **101**, 237801 (2008).
[24] M. Ravnik, M. Skarabot, S. Zumer, U. Tkalec, I. Poberaj, D. Babic, N. Osterman, and I. Musevic, Phys. Rev. Lett. **99**, 247801 (2007).
[25] C. Geuzaine and J.-F. Remacle, Int. J. Numer. Methods Eng. **79**, 1309 (2009).
[26] M. Tasinkevych, N. M. Silvestre, and M. M. T. da Gama, New J. Phys. **14**, 073030 (2012).
[27] W. H. Press, S. A. Teukolsky, W. T. Vetterling, and B. P. Flannery, *Numerical Recipes*, 2nd ed. (Cambridge University Press, Cambridge, 1992).